Missouri University of Science and Technology
Scholars' Mine

Chemical and Biochemical Engineering Faculty Research & Creative Works

Linda and Bipin Doshi Department of Chemical and Biochemical Engineering

17 May 2013

Increasing Round Trip Efficiency of Hybrid Li-air Battery with Bifunctional Catalysts

Kan Huang

Yunfeng Li

Yangchuan Xing
Missouri University of Science and Technology, XingY@Missouri.edu

Follow this and additional works at: https://scholarsmine.mst.edu/che_bioeng_facwork

 Part of the Biochemical and Biomolecular Engineering Commons

Recommended Citation

K. Huang et al., "Increasing Round Trip Efficiency of Hybrid Li-air Battery with Bifunctional Catalysts," *Electrochimica Acta*, vol. 103, pp. 44 - 49, Elsevier; International Society of Electrochemistry (ISE), May 2013.
The definitive version is available at https://doi.org/10.1016/j.electacta.2013.04.027

This Article - Journal is brought to you for free and open access by Scholars' Mine. It has been accepted for inclusion in Chemical and Biochemical Engineering Faculty Research & Creative Works by an authorized administrator of Scholars' Mine. This work is protected by U. S. Copyright Law. Unauthorized use including reproduction for redistribution requires the permission of the copyright holder. For more information, please contact scholarsmine@mst.edu.

Electrochimica Acta 103 (2013) 44–49

Contents lists available at SciVerse ScienceDirect

Electrochimica Acta

journal homepage: www.elsevier.com/locate/electacta

Increasing round trip efficiency of hybrid Li–air battery with bifunctional catalysts

Kan Huang [a], Yunfeng Li [b], Yangchuan Xing [b,*]

[a] Department of Chemical and Biological Engineering, Missouri University of Science and Technology, Rolla, MO 65401, United States
[b] Department of Chemical Engineering, University of Missouri, Columbia, MO 65211, United States

ARTICLE INFO

Article history:
Received 29 January 2013
Received in revised form 30 March 2013
Accepted 2 April 2013
Available online 17 April 2013

Keywords:
Round trip efficiency
Li–air battery
Sulfuric acid electrolyte
Bifunctional catalyst
Oxygen evolution

ABSTRACT

Previously it was shown that Pt as cathode catalyst has a large overpotential during charge in rechargeable hybrid Li–air battery with sulfuric acid catholyte. This article demonstrates that a bifunctional catalyst composed of Pt and IrO_2 supported on carbon nanotubes can address this problem. The specially designed and synthesized bifunctional catalyst showed significant overpotential reduction and achieved a round trip energy efficiency of 81% after 10 cycles, higher than many achieved in aprotic Li–O_2 batteries. The hybrid Li–air battery was discharged and recharged for 20 cycles at 0.2 mA/cm^2, showing a fairly stable cell performance. A specific capacity of 306 mAh/g and a specific energy of 1110 Wh/kg were obtained for the hybrid Li–air battery in terms of acid weight.

© 2013 Elsevier Ltd. All rights reserved.

1. Introduction

Lithium–air battery (LAB) has attracted intensive attention due to their high theoretical energy densities, comparable to that of gasoline [1–3]. Since Abraham and Jiang [4] proposed rechargeable non-aqueous lithium–oxygen battery, major efforts have been paid on aprotic electrolytes [5–7]. A major problem with aprotic LAB is that the insoluble discharge products, lithium oxides, deposit in the porous cathode and block further oxygen intake. Consequently, discharge ends quickly when the pores are clogged. The insulating nature of lithium oxides also lead to sudden drop of output voltage, increase of charge potential, and thus loss of capacity [1]. In addition, contamination of moisture in aprotic electrolytes can degrade lithium metal, causing self-charging and circuit shortening [8,9].

The development of an aqueous version of LAB has opened an alternative way to aprotic LAB [10]. The current LAB involves using hybrid electrolytes including a Li-ion conducting, electronically insulating membrane, such as LISICON-type glass, that is impermeable to liquid electrolytes and can protect the Li metal from direct contact with aqueous catholytes [2]. Such hybrid electrolyte LABs (HyLABs) have been demonstrated in aqueous neutral [11], acidic [12,13] and alkaline electrolytes in the cathodes [14,15]. Water is reduced in neutral or basic electrolytes when batteries are discharged, which follows $O_2 + 2H_2O + 4e^- \rightarrow 4OH^-$ ($E^0 = 0.4$ V *vs.* RHE), yielding a theoretical voltage at 3.43 V. In acidic electrolytes, oxygen is reduced through $O_2 + 4H^+ + 4e^- \rightarrow 2H_2O$ ($E^0 = 1.23$ V *vs.* RHE) which produces a 4.27 V theoretical voltage.

To date, Pt is still the most active catalyst for oxygen reduction reaction (ORR) [16–18], even though metal free N-doped graphene [19], manganese oxides [15] and perovskite oxides [20] were reported to exhibit some ORR activities. Pt is most suitable for use in acids for stability, and there are several studies reporting utilizing Pt as ORR catalyst in acid based LAB. Zhang et al. [12] reported using Pt mesh as cathode catalyst in acetic acid, demonstrating 15 charge–discharge cycles. Li et al. [21] used 40 wt.% Pt/C in phosphoric acid electrolyte and observed a potential difference increasing from 1.0 to 1.3 V after 20 cycles. In order to reverse a discharged LAB to its original charged state, an extra overpotential, usually positive 200–300 mV to the standard $E^0 = 1.23$ V, is required to electrolyze water for OER [22]. Under this overpotential, Pt is oxidized to form an oxide film and lose its catalytic ability [23,24]. Our previous work [25] has demonstrated sulfuric acid as catholyte in a HyLAB. The cathode catalyst was also Pt but supported on carbon nanotubes (CNTs) with ultralow Pt loading at only 5×10^{-5} g/cm^2. While a discharge specific energy achieved was over 1000 Wh/kg, the round trip efficiency was low due to the large overpotential gap between charge and discharge. It was concluded that a bifunctional electrocatalyst is needed to reduce overpotential for OER.

The limited resource of iridium makes it an expensive element to be used in large quantity in any practical applications. Nevertheless, iridium oxide (IrO_2) has been found to be an active and stable OER catalyst at high current densities [26–31]. Pt/IrO_2 as a bifunctional

* Corresponding author. Tel.: +1 573 884 1067.
E-mail address: xingy@missouri.edu (Y. Xing).

0013-4686/$ – see front matter © 2013 Elsevier Ltd. All rights reserved.
http://dx.doi.org/10.1016/j.electacta.2013.04.027

oxygen catalyst has been used in regenerative fuel cells [32–34], in which Pt serve for ORR and IrO_2 for OER. But such catalysts are often composed of large size of IrO_2 particles. In addition, carbon black is often used as the support. Here, we report a fundamental study on developing a CNT-supported Pt/IrO_2 bifunctional oxygen catalyst that is prepared in a unique thermal oxidation technique. Used for the HyLAB, it was shown that the round trip efficiency can be much improved by using the bifunctional oxygen catalyst.

2. Experimental

2.1. Preparation of bifunctional catalyst

CNTs (Nano Lab, 50 ± 15 nm) were treated with 3:1 H_2SO_4/HNO_3 (volume ratio) in an ultrasonic bath at 60 °C for 2 h for surface functionalization [35], followed by filtration and thorough washing with deionized water. 10 mg of the functionalized CNTs were then dispersed in 10 ml ethylene glycol plus 5 ml deionized water with the aid of sonication and stirring. Pre-determined amount of 0.01 M K_3IrCl_6 (Alfa Aesar) salt solution was pipetted into the above suspension and it was stirred under reflux conditions for reactions for 2 h. The iridium salt was reduced to metallic Ir to form Ir nanoparticles deposited on the CNTs (Ir/CNTs), which were separated out with a centrifuge. The product was thoroughly washed and dried at 80 °C in a vacuum oven overnight. It was then annealed in air at 400 °C for 2 h to oxidize the metallic Ir nanoparticles into crystalline iridium oxide (IrO_2), leading to a final 10 wt.% IrO_2 loading on the CNTs. That catalyst was further made into a suspension, and deposition of 5 wt.% Pt on IrO_2/CNTs was achieved by a polyol process reported previously [36] to produce bifunctional catalyst Pt/IrO_2/CNTs. Using bare CNTs, Pt was also deposited on CNTs to make Pt/CNTs without iridium oxides.

2.2. Catalyst characterization

Morphologies of the catalysts were examined by transmission electron microscope (TEM) (FEI Tecnai F20). The crystalline phase of the catalysts was analyzed by X-ray diffraction (XRD) equipped with Cu K(α) and the XRD data were collected with a Philips X-Pert Diffractometer over an angle range of 2θ = 10–90° at a scanning rate of 0.026° s^{-1}.

All electrochemical experiments were performed with an Electrochemical Workstation (Bioanalytical Sciences, BAS 100). The working electrode was a glassy carbon rotating disk electrode (RDE) with a disk diameter at 5 mm (Gamry RDE 710). A Pt wire was used as the counter electrode and saturated Ag/AgCl as a reference electrode. The catalyst powder was dispersed in deionized water by sonication for 20 min to form 1 mg/mL catalyst suspension. 20 μL of the suspension was pipetted onto the disk and dried in air. About 5 μL Nafion solution (0.05 wt.%, Alfa Aesar) was then put on top of the catalyst. Cyclic voltammetry (CV) and OER measurements were carried out in N_2 purged 1.0 M H_2SO_4 at potential range of 0–1.5 V and 0.8–1.6 V (*vs.* RHE), respectively. ORR measurement was taken in an O_2-saturared 1.0 M H_2SO_4 at rotating speed of 1600 rpm between 0.2 and 1.0 V (*vs.* RHE). To study the durability of Pt/IrO_2/CNTs, CV was conducted in N_2-bubbled 1.0 M H_2SO_4 in the potential range between 0.6 and 1.5 V (*vs.* RHE) up to 1000 cycles. The initial and final CV and ORR behaviors were recorded. For comparison, Pt/CNTs catalyst was also tested under the same cycling conditions. Current densities are calculated based on the total catalyst weight normalized to mA/mg.

2.3. Li–air cell testing

Details of air cathode preparation and cell assembly were reported in our previous work [25]. Tests of the cell were performed in an ambient environment and at room temperature. An Arbin battery test station (GT2000) was used for charge–discharge data collection. 0.01 mA/cm^2, 0.2 mA/cm^2, 0.5 mA/cm^2, and 1.0 mA/cm^2 discharge current densities were chosen for cell test in 1.0 M sulfuric acid. For long-term discharge and charge experiments, 0.2 mA/cm^2 current density was used. In this work, Pt/CNTs and Pt/IrO_2/CNTs were compared to demonstrate the advantage of the bifunctional catalyst.

3. Results and discussion

3.1. Catalysts and their characterization

Crystalline information of the catalyst was obtained from X-ray diffraction. XRD patterns of IrO_2/CNTs and Pt/IrO_2/CNTs were shown in Fig. 1. The absence of Ir metal diffraction and the presence of characteristic peaks belonging to rutile IrO_2 [22] in IrO_2/CNTs indicate complete transformation of metallic Ir to crystalline IrO_2. After Pt deposition, the crystalline form of IrO_2 remains unchanged in the catalyst. The peak at *ca.* 26° is ascribed to graphite, from the graphitic structure of the CNT support [36]. Fig. 2(A) shows a TEM image of the IrO_2/CNTs. It can be seen that the nanotube surface was uniformly covered with IrO_2 particles, and despite some in agglomerates there are no apparent sintering so that their nanoparticulate entity is retained after transformation. The two-step procedure was designed to uniformly deposit Ir on the CNTs first, and then convert it to IrO_2. This method can guarantee the uniform dispersion of IrO_2 with minimum aggregation and maximize the utilization of the active oxide surface.

The mean size of IrO_2 was measured to be 3.6 ± 0.5 nm from image analysis. A high magnification image in Fig. 2(A) shows lattice spacing of the graphitic layers of CNTs and rutile IrO_2 at 0.34 and 0.26 nm, respectively. The former is characteristic of basal planes in graphite, and the latter is characteristic of the (1 0 1) planes in rutile IrO_2, which also showed up in the XRD patterns as seen in Fig. 1. After deposition of Pt on IrO_2/CNTs, the morphology of IrO_2 does not show changes, as can be gauged from Fig. 2(B). XRD patterns (see Fig. 1) show that Pt now appears in the catalyst. Carefully examining the surface of the catalyst Pt/IrO_2/CNTs, there exist many round darker black nanoparticles. These nanoparticles are believed to be Pt since stronger lattice diffraction occurs in metals than in oxides,

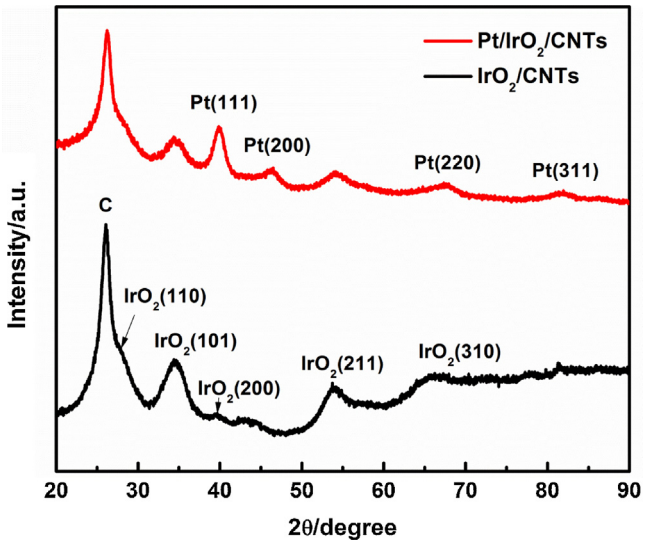

Fig. 1. X-ray diffraction patterns of catalysts IrO_2/CNTs and Pt/IrO_2/CNTs, showing a rutile IrO_2 and fcc Pt supported on carbon nanotubes. For clarity, the IrO_2 peaks are not marked on the pattern of catalyst Pt/IrO_2/CNTs.

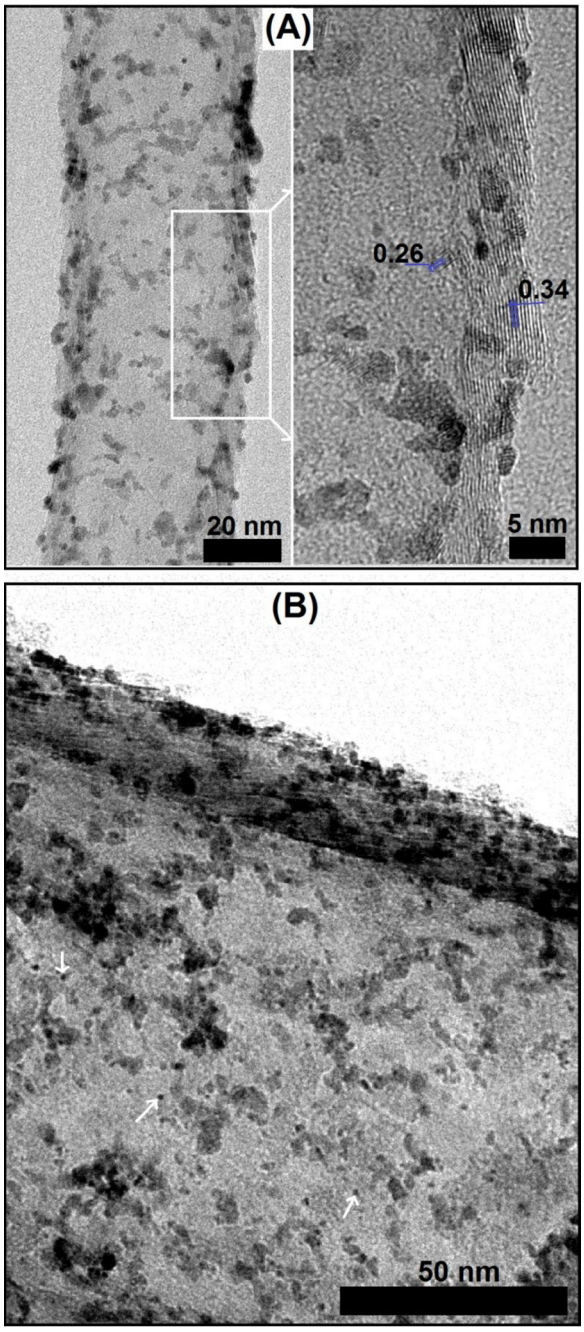

Fig. 2. TEM images of (A) IrO_2/CNT; shown are a low and a high magnification images. The numbers on the right image are lattice spacing (in nm), with 0.34 nm for graphite and 0.26 nm corresponding to rutile IrO_2 crystalline plane (1 0 1). (B) Pt/IrO_2/CNTs, showing the round dark black dots as Pt nanoparticles (*e.g.*, those indicated by arrows); no obvious morphological changes of the IrO_2 particles were observed.

giving the contrast. These nanoparticles are measured to have a size of 2.3 ± 0.2 nm.

3.2. Electrochemical properties of the bifunctional catalyst

The prepared catalysts were put under electrochemical tests in a three-electrode cell. The CV plots of catalysts Pt/CNTs, IrO_2/CNTs and Pt/IrO_2/CNTs were presented in Fig. 3(A). The anodic peak at 0.66 V and cathodic peak at 0.58 V were associated with the redox reactions of surface oxide groups, which have been found in acid-treated CNTs [35]. The anodic current occurred beyond 1.4 V (*vs.* RHE) was assigned to water oxidation currents [22]. IrO_2 was found to be electrochemically inert in the potential range of 0–1.4 V and have negligible contribution to the electrochemical surface area (ESA), while Pt/IrO_2/CNTs exhibits the typical peaks belonging to hydrogen ad/de-sorption on Pt surface [36]. The ESA of Pt in the catalyst was obtained using the methods commonly accepted [36,37]. The ESA in Pt/IrO_2/CNTs was obtained to be 905.7 cm^2/mg_{Pt}, close to the 996.2 cm^2/mg_{Pt} obtained for Pt/CNTs, indicating that Pt active surface area is large in both catalysts.

The ORR activities of IrO_2/CNT, Pt/CNT and Pt/IrO_2/CNTs were plotted in Fig. 3(B). IrO_2/CNTs exhibits negligible catalytic activity and has no contribution toward ORR. Meanwhile, Pt/IrO_2/CNTs showed a similar ORR performance as Pt/CNTs with the same Pt loading, suggesting that IrO_2 has not affected Pt for catalyzing ORR. Linear sweep voltammetry (LSV) was conducted to record the OER performances of the three different catalysts. As shown in Fig. 3(C), Pt has some catalytic activity toward OER (all OER currents were capacitance-corrected [22]), but is significantly lower when compared to that from IrO_2. The mass activity of IrO_2/CNTs at overpotential $\eta = 0.25$ V can reach 6 A/g_{IrO_2} without Ohmic correction, which are comparable or better than the 5 A/g_{IrO_2} and 3 A/g_{IrO_2} reported by Rasten et al. [29] and Lee et al. [22], respectively, at the same overpotential. We found that by incorporating Pt with IrO_2/CNTs, a significantly higher current density can be achieved than IrO_2/CNTs alone (96 $mA/mg_{catal.}$ *vs.* 56 $mA/mg_{catal.}$ at 1.6 V), which is also higher than the sum of IrO_2/CNTs and Pt/CNTs, indicative of that there may be a possible synergistic effect between Pt and the oxide IrO_2 for OER. A similar enhancement was observed by Yao et al. who used Pt supported on pure IrO_2 [33]. It was argued that the downshift of *d*-band center of Pt on Pt/IrO_2 weakened the O_{ads} bound to the catalytic surface, favoring water dissociation to form oxygen. It decreases the coverage of O_2/O_{ads} on the catalyst surface and thus, increases the available active sites.

To gain information about the stability of the catalyst Pt/IrO_2/CNTs, accelerated cycling test was performed by applying 1000 potential cycles from 0.6 to 1.5 V (*vs.* RHE) in N_2-bubbled 1.0 M H_2SO_4. As shown in Fig. 4(A), Pt in this catalyst only suffered very small surface area loss, verified by negligible change in H ad/de-sorption region of 0.05–0.4 V before and after the potential cycling tests. In contrast, ESA of Pt/CNTs suffered a much larger loss after 1000 cycles, from 996 to 230 cm^2/mg_{Pt}, leading to a severe degradation of ORR performances. Fig. 4(B) shows that the ORR half-wave potential shifted 40 mV negatively, indicative of an ORR activity loss, but it is much smaller than that of the Pt/CNT catalyst (*ca.* 300 mV shift). We attributed the loss of the Pt to its easy degradation on carbon support due to weak interaction between the metal and carbon. We have previously shown that Pt severely degrades on carbon black (Vulcan-XC72) in sulfuric acid, but it can be significantly improved by supporting the Pt on a conducting titanium suboxide coated on the CNTs [38]. The fact that oxide IrO_2 is involved may have similarly improved the stability of Pt, although perhaps to lesser degree since iridium oxide in this case is a not a continuous film and some Pt is in contact with carbon. Decrease in ORR activity is also attributed to the formation of a thin Pt-oxide layer at high potentials. Reier et al. [39] observed electrochemical activity of Pt nanoparticle surface despite deactivation by forming an oxide layer, which is believed to be responsible for the observed ORR activity in this work.

In the OER region (1.4–1.6 V), the CVs showed changes of the catalyst Pt/IrO_2/CNTs after cycling. It was determined that the OER current density decreased from 105 to 86 $mA/mg_{catal.}$ at 1.6 V (see Fig. 4(C)). Kötz et al. [40] proposed a mechanism for OER on iridium oxide. Oxygen is split off from water on IrO_3 with Ir in the hexavalent state, which was formed by two consecutive deprotonation steps from $IrO(OH)_2$. Meanwhile, IrO_3 may corrode into electrolyte as IrO_4^{2-} ion and lead to direct OER activity loss. Formation of

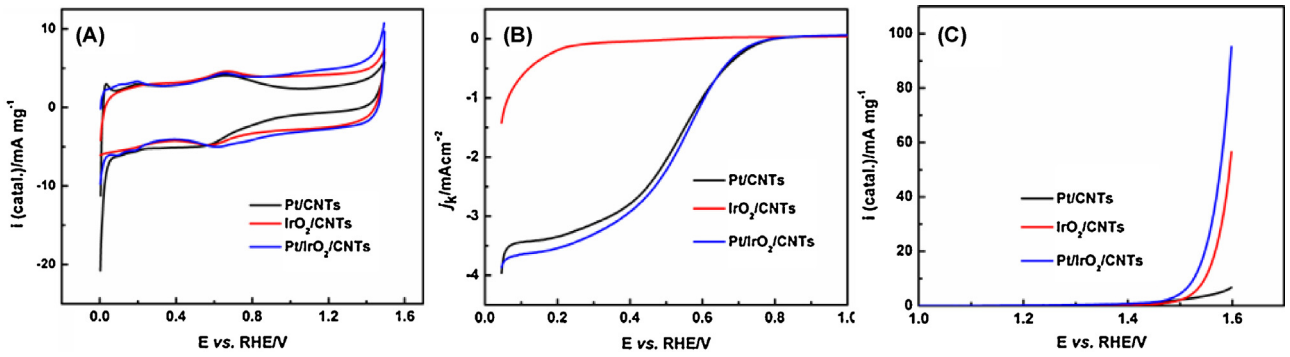

Fig. 3. Electrochemical characterizations of catalysts. (A) Cyclic voltammetry curves of Pt/CNTs, IrO_2/CNTs and Pt/IrO_2/CNTs. (B) Polarization curves of ORR on Pt/CNTs, IrO_2/CNTs and Pt/IrO_2/CNTs. (C) Polarization curves of OER on Pt/CNTs, IrO_2/CNTs and Pt/IrO_2/CNTs.

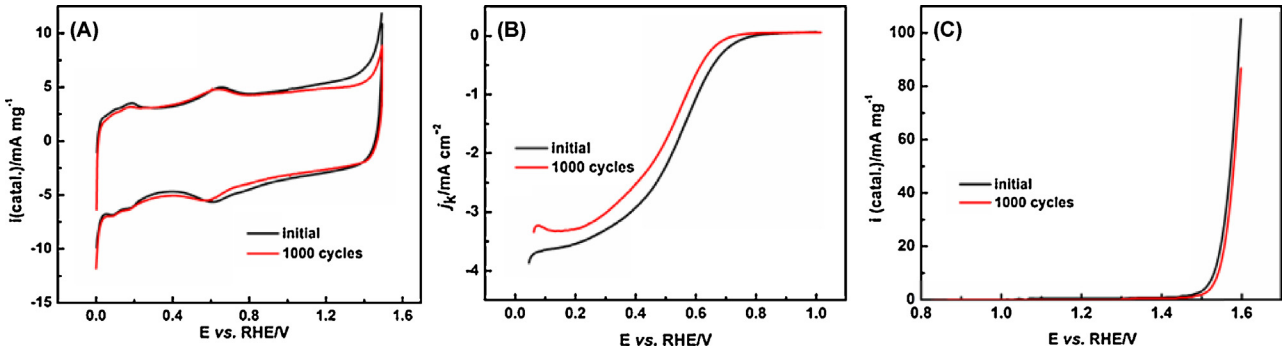

Fig. 4. Electrochemical characterizations of catalyst Pt/IrO_2/CNTs before and after 1000 cycles. (A) Cyclic voltammetry curves. (B) Polarization curves of ORR. (C) OER activities.

poorly conductive and catalytically inactive Pt oxide species may also contribute to the loss of OER activity [39]. Nevertheless, the results showed a relatively stable performance of the bifunctional catalyst in sulfuric acid electrolyte.

3.3. Li–air cell performance

Fig. 5 presents the discharge of a full Li–air cell using Pt/CNTs or Pt/IrO_2/CNTs as catalysts in the cathode at different discharge current densities. The operation potentials dropped from 3.72 to 3.21 V with increasing current densities from 0.1 to 1.0 mA/cm^2,

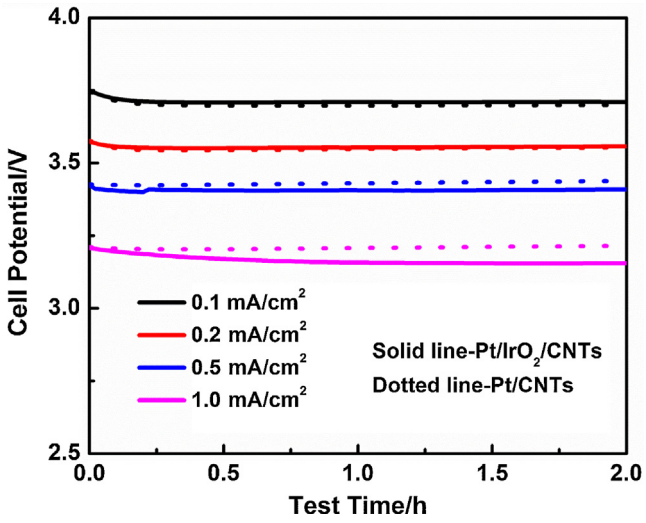

Fig. 5. Performance in discharge of Li–air cells catalyzed by Pt/CNTs and Pt/IrO_2/CNTs at different current densities.

and this polarization was mainly due to the internal resistance at the anode side [12,25]. At 0.1–0.5 mA/cm^2 discharge current densities, the cell performance with Pt/CNTs or Pt/IrO_2/CNTs is very close as seen from Fig. 5, indicative of that there are no significant catalytic differences between Pt/CNTs and Pt/IrO_2/CNTs toward ORR. This observation supports the findings that IrO_2 has negligible contribution to ORR. However, at a higher current density (*e.g.*, 1.0 mA/cm^2), Pt/CNTs yielded a slightly better performance than Pt/IrO_2/CNTs. Similar findings were reported previously, showing that Pt black is better than Pt/IrO_x in regenerative fuel cells [33,41]. As shown in Fig. 2(B), some Pt nanoparticles were found to be on the IrO_2 surface rather than directly deposited on the CNTs. We assume that some electron conducting path maybe hindered by the less conductive IrO_2 agglomerates because the ohmic resistance of IrO_2 is nearly five times larger than that of Pt [33]. Under a high current density, the inefficiency of electron transport could result in a voltage loss.

Cycling results of the Li–air cell with Pt/CNTs or Pt/IrO_2/CNTs at 0.2 mA/cm^2 are presented in Fig. 6. The duration for charge and discharge was set at 1.5 h each, and the cell was cycled for 21 h. Using Pt/CNTs as the cathode catalyst, the potential gap between the charge and discharge was about 1.25 V initially, and it slowly increased to 1.45 V after 6 cycles, as shown in Fig. 6(A). A loss of the discharge potential was recorded from 3.50 to 3.36 V, indicative of that a higher overpotential was induced in order to initiate the ORR, attributed to surface oxide formation on Pt. It is well known that Pt is an excellent electrocatalyst for ORR but not one for OER, due to its high oxygen evolution overpotential and formation of a stable surface oxide layer [23]. The charge process requires a much higher potential to dissociate water into oxygen. The potential of the first recharge reached 4.75 V (*vs.* Li^+/Li), corresponding to an OER potential of 1.7 V (*vs.* RHE). Jerkiewicz et al. [24] suggested that Pt^{2+}–O^{2-} is formed above 1.15 V (*vs.* RHE), and the oxide film is not reduced until the potentials are near the H potential range [23]. The

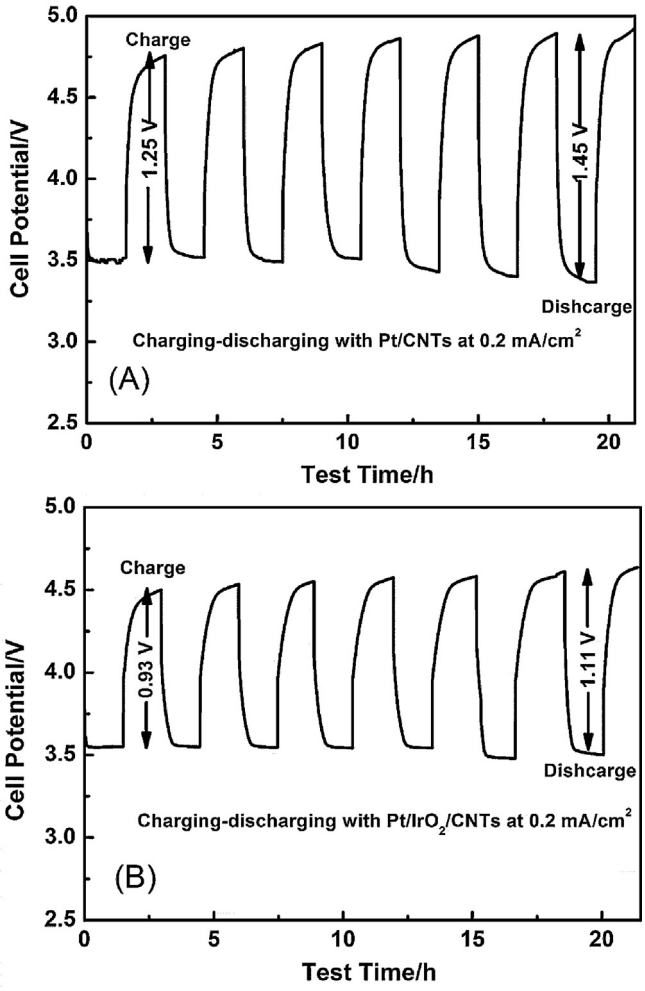

Fig. 6. Charge–discharge performance of the Li–air cells at 0.2 mA/cm^2 in 1.0 M H_2SO_4 with (A) cathode with Pt/CNTs, and (B) cathode with Pt/IrO_2/CNTs.

loss of activity of Pt is again attributed mainly to the formation of the surface oxide.

As discussed above, intensive scanning of Pt/CNTs in a high potential range has led to a dramatic ESA and ORR loss, thus the passivation of Pt may be one of the major factors responsible for the decrease of cell performance. It was found that the charge potential gradually increased in the first charge process, and this trend became more evident in the later charge steps. On the contrary, a decreasing tendency in discharge potential was found in the second and following discharge cycles. All those observations suggested that utilizing single Pt as cathode catalyst has its limitations and the cell could not sustain for stable charge–discharge cycles.

In the case of Pt/IrO_2/CNTs, the obvious degradation was alleviated as illustrated in Fig. 6(B). Each discharge/charge cycle exhibited flat potential curves and the corresponding potential gap at the beginning and after 6 cycles were 0.93 V and 1.11 V, respectively, showing much improved stability over Pt/CNTs. Throughout the entire cycling, the discharge potentials remained well at 3.5 V, similar to the discharging potential with catalyst Pt/CNTs. However, the charging potential stayed at around 4.5–4.6 V, approximately 0.25 V lower than that from charge with Pt alone. At lower OER overpotentials, Pt suffer less oxidation and thus form a thinner oxide layer, which may reduce the barrier to access active Pt surface for ORR. Consequently, the cell exhibited a much improved discharge performance. As an OER catalyst, IrO_2 not only decreases the charging overpotential, but also protects Pt from over-oxidation.

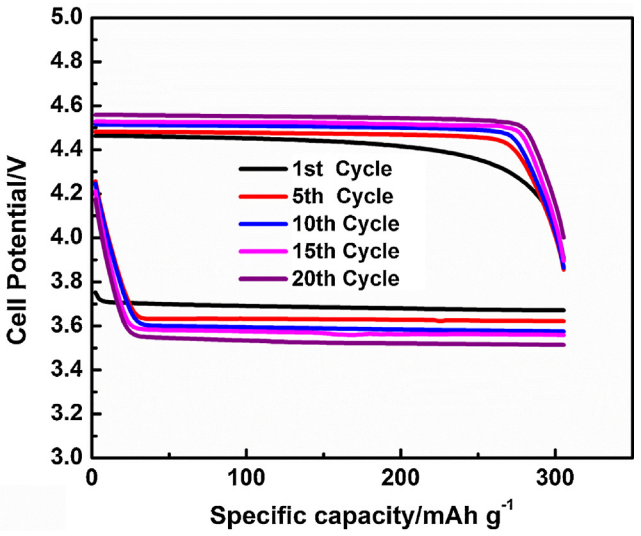

Fig. 7. Cycling performance of the Li–air cell catalyzed by Pt/IrO_2/CNTs at 0.2 mA/cm^2 in 0.01 M H_2SO_4 catholyte.

The Li ion conducting ceramic glass membrane (O'Hara) was reported to be unstable in strong acidic and basic media [42]. To avoid corrosion of the glass membrane and investigate the cell performance catalyzed by the bifunctional catalyst for an extended period, we further conducted cell testing for discharge/charge in diluted 0.01 M H_2SO_4. Our previous work has found that this concentration of sulfuric acid did not notably impact cell performance [25]. For this study, flat discharge–charge potential curves of Pt/IrO_2/CNTs at 0.2 mA/cm^2 were also found, illustrated in Fig. 7. In the first cycle, the discharge and charge potential were found at 3.68 V and 4.45 V, respectively. A slightly higher discharge potential was found than that in concentrated sulfuric acid. Sulfate ion adsorption on the Pt would block active surface and impose a negative electronic effect on the ORR kinetics [43]. In addition, Li ions also affect the Pt ORR in sulfuric acid [44]. More diluted sulfuric acid may alleviate this influence and lead to slightly better ORR activity.

Our previous work has demonstrated the possibilities to achieve a discharge specific capacity of 306 mAh/g and a specific energy of 1067 Wh/kg after 75 h (based on the weight of sulfuric acid) [25]. To keep the same capacity, the discharging capacity in the current study was also cut off at 306 mAh/g. Again, the acid was found to have a 56% utilization of the theoretical capacity of 547 mAh/g, and the specific energy density at first discharge was measured at 1110 Wh/kg. The round trip efficiency is at 81% for the 10th cycle (84% for the 1st cycle). This round trip efficiency is higher than that (72%) we obtained previously [25]; it is also much higher than reported values (*e.g.*, 65%) in aprotic Li–O_2 cells [1].

After 20 cycles, the charge potential raised 100 mV to 4.55 V. The potential gap between charge and discharge increased to 1.02 V, but it is much smaller than those in concentrated acids, as expected. The mild degradation of cell performance may come from the impedance change caused by the glass membrane and inevitable oxidation of Pt metal. In the case of Pt/CNTs [25], the potential gap increased quickly from 0.89 to 1.37 V after 10 cycles, demonstrating the bifunctional catalyst has significantly reduced the overpotential in the aqueous Li–air battery, increasing its round trip efficiency and rechargeability. Rechargeability is a significant issue in secondary Li–air battery. Most recently, Peng et al. [45] reported a highly reversible non-aqueous Li–air battery with a low potential gap (0.5–0.6 V) using dimethyl sulfoxide electrolyte and a porous gold electrode. Nevertheless, some fundamental technical challenges remain in both aqueous and organic Li–air batteries, and

more research needs to be conducted to achieve a practical cell performance.

4. Conclusions

In summary, we have successfully developed a bifunctional catalyst, Pt/IrO_2/CNTs, for Li–air battery using sulfuric acid as catholyte. The catalyst exhibits excellent catalytic activities with smaller OER overpotentials, higher OER activity, and better electrochemical stability. Compared to mono Pt catalyst, the introduction of the bifunctional catalyst significantly reduced the charge voltage by more than 300 mV, and thus increased its round trip efficiency from 72% to 81% (evaluated at the 10th cycle) for mono Pt and bifunctional catalyst, respectively. The hybrid Li–air battery can be cycled for 20 times without significant degradation. Discharge capacity of 306 mAh/g and specific energy of 1110 Wh/kg were demonstrated for the battery.

Acknowledgments

Financial support by the U.S. Department of Energy ARPA-E grant DEAR0000066 is gratefully acknowledged. We thank Max-Power, Inc. to supply the sealed anodes for our tests and NanoLab, Inc. to supply the carbon nanotubes. We also thank Dr. Eric Bohannan for his help in the XRD analysis and Dr. Kai Song for taking TEM images.

References

[1] G. Girishkumar, B. McCloskey, A.C. Luntz, S. Swanson, W. Wilcke, Lithium–air battery: promise and challenges, Journal of Physical Chemistry Letters 1 (2010) 2193.
[2] P.G. Bruce, S.A. Freunberger, L.J. Hardwick, J.-M. Tarascon, Li–O_2 and Li–S batteries with high energy storage, Nature Materials 11 (2012) 19.
[3] J. Christensen, P. Albertus, R.S. Sanchez-Carrera, T. Lohmann, B. Kozinsky, R. Liedtke, J. Ahmed, J. Kojic, A critical review of Li/air batteries, Journal of the Electrochemical Society 159 (2012) R1.
[4] K.M. Abraham, Z. Jiang, A polymer electrolyte-based rechargeable lithium/oxygen battery, Journal of the Electrochemical Society 143 (1996) 1.
[5] J. Read, Characterization of the lithium/oxygen organic electrolyte battery, Journal of the Electrochemical Society 149 (2002) A1190.
[6] J. Read, Ether-based electrolytes for the lithium/oxygen organic electrolyte battery, Journal of the Electrochemical Society 153 (2006) A96.
[7] W. Xu, J. Xiao, D. Wang, J. Zhang, J.-G. Zhang, Crown ethers in nonaqueous electrolytes for lithium/air batteries, Electrochemical and Solid-State Letters 13 (2010) A48.
[8] D. Aurbach, Review of selected electrode–solution interactions which determine the performance of Li and Li ion batteries, Journal of Power Sources 89 (2000) 206.
[9] K. Xu, Nonaqueous liquid electrolytes for lithium-based rechargeable batteries, Chemical Reviews 104 (2004) 4303.
[10] S.J. Visco, B.D. Katz, Y.S. Nimon, L.C.D. Jonghe, Protected active metal electrode and battery cell structure with non-aqueous interlayer architecture, U.S. Patent 7,282,295, 2007.
[11] T. Zhang, N. Imanishi, S. Hasegawa, A. Hirano, J. Xie, Y. Takeda, O. Yamamoto, N. Sammes, Li/polymer electrolyte/water stable lithium-conducting glass ceramics composite for lithium–air secondary batteries with an aqueous electrolyte, Journal of the Electrochemical Society 155 (2008) A965.
[12] T. Zhang, N. Imanishi, Y. Shimonishi, A. Hirano, Y. Takeda, O. Yamamoto, N. Sammes, A novel high energy density rechargeable lithium/air battery, Chemical Communications 46 (2010) 1661.
[13] T. Zhang, N. Imanishi, Y. Shimonishi, A. Hirano, J. Xie, Y. Takeda, O. Yamamoto, N. Sammes, Stability of a water-stable lithium metal anode for a lithium–air battery with acetic acid–water solutions, Journal of the Electrochemical Society 157 (2010) A214.
[14] P. He, Y. Wang, H. Zhou, A Li–air fuel cell with recycle aqueous electrolyte for improved stability, Electrochemistry Communications 12 (2010) 1686.
[15] Y. Wang, H. Zhou, A lithium–air battery with a potential to continuously reduce O_2 from air for delivering energy, Journal of Power Sources 195 (2010) 358.
[16] Y. Xing, Y. Cai, M.B. Vukmirovic, W.-P. Zhou, H. Karan, J.X. Wang, R.R. Adzic, Enhancing oxygen reduction reaction activity via Pd–Au alloy sublayer mediation of Pt monolayer electrocatalysts, Journal of Physical Chemistry Letters 1 (2010) 3238.
[17] J. Zhang, M.B. Vukmirovic, K. Sasaki, A.U. Nilekar, M. Mavrikakis, R.R. Adzic, Mixed-metal Pt monolayer electrocatalysts for enhanced oxygen reduction kinetics, Journal of the American Chemical Society 127 (2005) 12480.
[18] H.A. Gasteiger, S.S. Kocha, B. Sompalli, F.T. Wagner, Activity benchmarks and requirements for Pt, Pt-alloy, and non-Pt oxygen reduction catalysts for PEMFCs, Applied Catalysis B: Environmental 56 (2005) 9.
[19] E. Yoo, H. Zhou, Li–air rechargeable battery based on metal-free graphene nanosheet catalysts, ACS Nano 5 (2011) 3020.
[20] J. Suntivich, H.A. Gasteiger, N. Yabuuchi, Y. Shao-Horn, Electrocatalytic measurement methodology of oxide catalysts using a thin-film rotating disk electrode, Journal of the Electrochemical Society 157 (2010) B1263.
[21] L. Li, X. Zhao, A. Manthiram, A dual-electrolyte rechargeable Li–air battery with phosphate buffer catholyte, Electrochemistry Communications 14 (2012) 78.
[22] Y. Lee, J. Suntivich, K.J. May, E.E. Perry, Y. Shao-Horn, Synthesis and activities of rutile IrO_2 and RuO_2 nanoparticles for oxygen evolution in acid and alkaline solutions, Journal of Physical Chemistry Letters 3 (2012) 399.
[23] B.E. Conway, T.C. Liu, Characterization of electrocatalysis in the oxygen evolution reaction at platinum by evaluation of behavior of surface intermediate states at the oxide film, Langmuir 6 (1990) 268.
[24] G. Jerkiewicz, G. Vatankhah, J. Lessard, M.P. Soriaga, Y.-S. Park, Surface-oxide growth at platinum electrodes in aqueous H_2SO_4: reexamination of its mechanism through combined cyclic-voltammetry, electrochemical quartz-crystal nanobalance, and Auger electron spectroscopy measurements, Electrochimica Acta 49 (2004) 1451.
[25] Y. Li, K. Huang, Y. Xing, A hybrid Li–air battery with buckypaper air cathode and sulfuric acid electrolyte, Electrochimica Acta 81 (2012) 20.
[26] L. Ouattara, S. Fierro, O. Frey, M. Koudelka, C. Comninellis, Electrochemical comparison of IrO_2 prepared by anodic oxidation of pure iridium and IrO_2 prepared by thermal decomposition of H_2IrCl_6 precursor solution, Journal of Applied Electrochemistry 39 (2009) 1361.
[27] S. Song, H. Zhang, X. Ma, Z. Shao, R.T. Baker, B. Yi, Electrochemical investigation of electrocatalysts for the oxygen evolution reaction in PEM water electrolyzers, International Journal of Hydrogen Energy 33 (2008) 4955.
[28] R.E. Fuentes, J. Farell, J.W. Weidner, Multimetallic electrocatalysts of Pt, Ru, and Ir supported on anatase and rutile TiO_2 for oxygen evolution in an acid environment, Electrochemical and Solid-State Letters 14 (2011) E5.
[29] E. Rasten, G. Hagen, R. Tunold, Electrocatalysis in water electrolysis with solid polymer electrolyte, Electrochimica Acta 48 (2003) 3945.
[30] M. Yagi, E. Tomita, T. Kuwabara, Remarkably high activity of electrodeposited IrO_2 film for electrocatalytic water oxidation, Journal of Electroanalytical Chemistry 579 (2005) 83.
[31] R. Tunold, A.T. Marshall, E. Rasten, M. Tsypkin, L.-E. Owe, S. Sunde, Materials for electrocatalysis of oxygen evolution process in PEM water electrolysis cells, ECS Transactions 25 (2010) 103.
[32] T. Ioroi, N. Kitazawa, K. Yasuda, Y. Yamamoto, H. Takenaka, Iridium oxide/platinum electrocatalysts for unitized regenerative polymer electrolyte fuel cells, Journal of the Electrochemical Society 147 (2000) 2018.
[33] W. Yao, J. Yang, J. Wang, Y. Nuli, Iridium oxide/platinum electrocatalysts for unitized regenerative polymer electrolyte fuel cells, Electrochemistry Communications 9 (2007) 1029.
[34] F.-D. Kong, S. Zhang, G.-P. Yin, N. Zhang, Z.-B. Wang, C.-Y. Du, Pt/porous-IrO_2 nanocomposite as promising electrocatalyst for unitized regenerative fuel cell, Electrochemistry Communications 14 (2012) 63.
[35] Y. Xing, L. Li, C.C. Chusuei, R.V. Hull, Sonochemical oxidation of multiwalled carbon nanotubes, Langmuir 21 (2005) 4185.
[36] Y. Xing, Synthesis and electrochemical characterization of uniformly-dispersed high loading Pt nanoparticles on sonochemically-treated carbon nanotubes, Journal of Physical Chemistry B 108 (2004) 19255.
[37] L. Li, Y. Xing, Pt–Ru nanoparticles supported on carbon nanotubes as methanol fuel cell catalysts, Journal of Physical Chemistry C 111 (2007) 2803.
[38] K. Huang, K. Sasaki, R.R. Adzic, Y. Xing, Increasing Pt oxygen reduction reaction activity and durability with a carbon-doped TiO_2 nanocoating catalyst support, Journal of Materials Chemistry 22 (2012) 16824.
[39] T. Reier, M. Oezaslan, P. Strasser, Electrocatalytic oxygen evolution reaction (OER) on Ru, Ir, and Pt catalysts: a comparative study of nanoparticles and bulk materials, ACS Catalysis 2 (2012) 1765.
[40] R. Kötz, H.J. Lewerenz, S. Stucki, XPS studies of oxygen evolution on Ru and RuO_2 anodes, Journal of the Electrochemical Society 130 (1983) 825.
[41] S.-D. Yim, W.-Y. Lee, Y.-G. Yoon, Y.-J. Sohn, G.-G. Park, T.-H. Yang, C.-S. Kim, Optimization of bifunctional electrocatalyst for PEM unitized regenerative fuel cell, Electrochimica Acta 50 (2004) 713.
[42] S. Hasegawa, N. Imanishi, T. Zhang, J. Xie, A. Hirano, Y. Takeda, O. Yamamoto, Study on lithium/air secondary batteries—stability of NASICON-type lithium ion conducting glass–ceramics with water, Journal of Power Sources 189 (2009) 371.
[43] J.X. Wang, N.M. Markovic, R.R. Adzic, Kinetic analysis of oxygen reduction on Pt(1 1 1) in acid solutions: intrinsic kinetic parameters and anion adsorption effects, Journal of Physical Chemistry B 108 (2004) 4127.
[44] H. Liu, Y. Xing, Influence of Li ions on the oxygen reduction reaction of platinum electrocatalyst, Electrochemistry Communications 13 (2011) 646.
[45] Z. Peng, S.A. Freunberger, Y. Chen, P.G. Bruce, A reversible and higher-rate Li–O_2 battery, Science 337 (2012) 563.